ISSN 1063-7834, Physics of the Solid State, 2020, Vol. 62, No. 5, pp. 891–901. © Pleiades Publishing, Ltd., 2020.
Russian Text © The Author(s), 2020, published in Fizika Tverdogo Tela, 2020, Vol. 62, No. 5, pp. 789–798.

MAGNETISM

Study of Features of the Composition, Magnetic, and Crystal Structure of Barium Hexaferrite $BaFe_{12-x}Ti_xO_{19}$

V. V. Korovushkin[a], A. V. Trukhanov[a, b, *], V. G. Kostishin[a], I. M. Isaev[a], I. V. Shchetinin[a], N. M. Durov[a], A. Yu. Mironovich[a], I. O. Minkova[a], and K. A. Astapovich[b]

[a] *National University of Science and Technology MISIS, Moscow, 119049 Russia*

[b] *Scientific and Production Center of the National Academy of Sciences of Belarus for Materials Science, Minsk, 220072 Belarus*

** e-mail: truhanov86@mail.ru*

Received October 31, 2019; revised December 17, 2019; accepted December 24, 2019

Abstract—The features of the composition, crystal, and magnetic structure of Ti-substituted barium hexaferrite $BaFe_{12-x}Ti_xO_{19}$ ($0.25 \le x \le 1.5$) are studied by Mössbauer spectroscopy, vibration magnetometry, X-ray diffraction, and simultaneous thermal analysis. Bounded heterovalent isomorphism implemented by the scheme $2Fe^{3+} \rightarrow Ti^{4+} + Fe^{2+}$ while retaining the charge balance is established when Fe^{3+} ions are partially substituted with Ti^{4+} ions. An increase in the 3*d*-electron density and the presence of Fe^{2+} in $BaFe_{12-x}Ti_xO_{19}$ samples with $x = 1.5$ is detected by Mössbauer spectroscopy. The heterovalent isomorphic substitution limit is determined to be within $0.75 < x < 1.0$. Using Mössbauer spectroscopy and X-ray diffraction, the formation of titanium-contained phases at $x = 1.0$ whose content increases with the degree of substitution is shown. The data on the preferential distribution of substituent ions (Ti^{4+}) in the barium hexaferrite structure at the 12*k* and 2*b* sites are presented.

Keywords: hexaferrites, heterovalent substitution, titanium, Mössbauer spectroscopy, magnetic properties, X-ray diffraction, simultaneous thermal analysis

DOI: 10.1134/S1063783420050145

1. INTRODUCTION

Magnetic properties of barium hexaferrites depend on both the isomorphic impurity type and content in the structure, which makes it possible of not only to study their properties, but also to synthesize samples with tailored characteristics for practical applications.

M-type hexaferrites and their solid solutions have a crystal structure isomorphic to a natural mineral, i.e., magnetoplumbit $PbFe_{12}O_{19}$, which was first studied by Adelskold [1].

Iron ions in the hexaferrite with such a structure are localized at five nonequivalent crystallographic sites: 2*a*, 2*b*, $4f_1$, $4f_2$, and 12*k*. Among them 2*a*, $4f_2$, and 12*k* are octahedral, $4f_1$ is tetrahedral, and 2*b* form a bipyramid. Polyhedra $4f_1$ and 2*a* are arranged in the spinel block (*S*), $4f_2$ and 2*b* are in the hexagonal block (*R*), and 12*k* is at the interface of spinel and hexagonal blocks (RS) [2].

In unsubstituted hexaferrite $BaFe_{12}O_{19}$, the collinear magnetic structure is implemented, in which magnetic moments of sites 12*k*, 2*a*, and 2*b* are directed to one side, while $4f_1$ and $4f_2$ are directed in antiparallel to the other side [3], which results in uncompensated antiferromagnetism (ferrimagnetism). Weakening of these interactions due to the substitution of Fe^{3+} ions of both groups with nonmagnetic and/or low-magnetic metal ions results in a decrease in the resulting magnetic moment and can lead to a noncollinear magnetic structure [4].

To controllably change magnetic and electrical properties, the principle of a change in the hexaferrite chemical composition is used.

In this case, most researchers considered the isovalent substitution of Fe^{3+} ions with metal ions with close ionic radius and an oxidation state of 3+, since the charge balance is implemented rather easily in this case (electrical neutrality law conservation) [5, 6]. The introduction of two or several various elements of the same valence also did not cause problems with charge balance, but complicates interpretation of their localization in the structure [7]. A much more complex situation arises for the charge balance if we consider heterovalent substitutions. Some authors, to provide the charge balance in the synthesis, use substitutions of Fe^{3+} ions with a $Me^{2+} + Me^{4+}$ pair. Substitutions with Ti^{4+} simultaneously with divalent ions Mn^{2+}, Co^{2+}, Zn, Ni were studied in many works. For example, in

[8], Fe^{3+} ions in strontium hexaferrite are substituted with Mn^{2+} + Ti^{4+} ions with the general crystallochemical formula $SrFe_{12-2x}Mn_x^{2+}Ti_x^{4+}O_{19}$. Although according to [8], Mn ions are localized at the site $4f_1$, there are different opinions on Ti^{4+} localization. A large number of studies are devoted to the study of barium hexaferrites alloyed with Ti^{4+} ions simultaneously with Co^{2+} ions, e.g., [9]. The results obtained show that the substitution of Fe^{3+} ions with Ti^{4+} ions simultaneously with Co^{2+} ions do not lead to a change in the hexaferrite structure, the charge balance in this case is retained, but the magnetization of samples decreases. In [9], it is believed that such materials can be used as radio absorbing ones.

Similar results leading to a decrease in the magnetizations as Ti^{4+} and Mg^{2+} ion pair is introduced into the structure are presented in [10] with an indicated increase in the unit cell parameter with the degree of substitution x. In the case of Fe^{3+} ion substitution with Ti^{4+} + Zn^{2+}, a higher isomorphic capacity of hexaferrites and the dependence of the saturation magnetization on methods and conditions of their synthesis are indicated in [11]. In [12], experiments on the introduction of three elements (Ti^{4+}, Mn^{2+}, Cu^{2+}) at $x = 1$, 2, and 3 into the lattice were performed; according to X-ray diffraction, hexaferrite was still single-phase at $x = 2$. However, the appearance of the second phase at $x = 2$ was detected in [13]. A decrease in the saturation magnetization and an increase in the permeability with x was indicated. An increase in the number of substituting ions to four resulted in ambiguity of results. In [14], it is believed that the obtained material with no agglomeration is applicable to high-frequency magnetic devices. In [15], even at $x = 0.5$, magnetic characteristics featured complex behavior as a result of the ambiguous cationic distribution of substituting elements in the structure. It should be noted that it is rather difficult to determine the cation localization at a large variety substituting ions; furthermore, it is difficult to determine the domination of any substituting ion on hexaferrite properties.

Since isovalent substitutions of Fe^{3+} ions with single elements and Me^{2+} + Me^{4+} pair are widely enough studied, it is of interest to consider heterovalent substitutions of Fe^{3+} ions separately with Me^{2+} and Me^{4+} ions. Few sources suggest that the isomorphic capacity of hexaferrite in the case of titanium introduction is slightly higher than for other elements, which extends the applicability of such hexaferrites in microwave techniques. Taking this into account, hexaferrite alloyed with Ti^{4+} ions was chosen for study.

Among early studies of titanium-alloyed barium hexaferrites is [16], in which a natural hexaferrite analogue of composition $BaFe_{10}Ti_2O_{19}$ found in Germany and approved as a new mineral Batiferrit was studied. Its composition, physical properties, and structure, which corresponded to the magnetoplumbit structure according to X-ray diffraction, were studied. In [17], the study of hexaferrites with $x = 0$, 0.6, 0.8, and 1.0 by X-ray diffraction and magnetometry showed a change in the unit cell parameters and titanium introduction into tetrahedral (17%) and octahedral (75%) sites, which leads to a decrease in the remanent magnetization and magnetic anisotropy with increasing Ti content. In this case, it is believed that the magnetization increases at low titanium concentrations and decreases with increasing titanium concentration.

A series of M-type barium hexaferrites was synthesized with partial substitution of Fe_2O_3 with TiO_2 in [18]. The melt composition (mol %) was $40BaO + 33B_2O_3 + (27 - x)Fe_2O_3 + xTiO_2$, where x = 0, 3.6, 5.4, and 7.2 mol % of TiO_2.

Substituted ferrites were studied using X-ray diffraction, Mössbauer spectroscopy, and magnetometry. The X-ray diffractions data showed that all samples, except for the ferrite phase, had a $BaTi_6O_{13}$ phase impurity. Mössbauer spectra of compositions with $x = 0$, 3.6, 5.4 mol % of TiO_2 showed magnetic ordering with strong line broadening. Furthermore, line broadening increased with the TiO_2 content. According to Mössbauer parameters, Ti^{4+} ions occupy sites $2a$ and $12k$; at high contents, the also occupy sites $2b$ and $4f_2$, which causes a decrease in the coercive force and saturation magnetization.

Single crystals of Ti-substituted barium hexaferrite $BaFe_{12-x}Ti_xO_{19}$ with $x < 1.3$ were studied in [19, 20]. The Ti distribution over various crystallographic sites was determined by the X-ray diffraction data. At low Ti contents (x to 0.8), the unit cell expands; as x further increases, the unit cell begin to constrict. This is associated with the Fe^{3+}-to-Fe^{2+} transition and vacancy formation to maintain the charge balance. In this case, the Curie temperature and magnetization monotonically decrease.

Literature sources show that there is no consensus on the cationic distribution in the hexaferrite structure and in particular on titanium localization. In some works, it is stated that Ti^{4+} ions can enter almost all sites except for $4f_1$ [18]; in others, its incorporation into site $2b$ is denied [17]. Questions also arise on the charge balance mechanism in hexaferrite when Ti^{4+} ions enter the lattice and the appearance of ions with an increased isomer shift to 0.49 mm/s, related immediately to Fe^{2+} ions [18], and the formation of additional phases, depending on the titanium concentration.

Therefore, the objective of this work is to study the correlation of chemical and phase composition and magnetic properties as functions of the preferential distribution of the heterovalent substituent ion in the $BaFe_{12-x}Ti_xO_{19}$ samples under study with $0.25 \le x \le 1.5$ in the implementation of the charge balance scheme.

2. OBJECTS AND METHODS OF STUDY

The objects of study were polycrystalline barium hexaferrite $BaFe_{12-x}Ti_xO_{19}$ samples, where $x = 0.25$, 0.5, 0.75, 1.0, 1.25, and 1.5. The samples were produced by the ceramic technology from ultrapure grade oxides Fe_2O_3, TiO_2, and carbonate $BaCO_3$. The preliminary initial composition was subjected to synthesizing annealing in air at 1200°C (6 h) and then was sintered at 1300°C (6 h). After sintering, samples were slowly cooled in a furnace (~100°/h) [13].

The Mössbauer spectra of $BaFe_{12-x}Ti_xO_{19}$ samples were measured using an Ms-1104 Em spectrometer with constant acceleration, the number of points of 512, a Co^{57} γ-radiation source in a chromium matrix, at room temperature. The isomer (chemical) shift was calculated with respect to α-Fe. Powder samples 0.05–0.07 mm in size made of sintered ferrite were used. The mathematical treatment of the spectra was performed by the Univem Ms program.

The magnetic parameters, i.e., the specific magnetization σ_s, remanent magnetization σ_r, coercive force H_c, and hysteresis loop shape, were measured using a VSM 250 vibration magnetometer in a magnetic field of 20 kOe at 300 K.

The Curie temperature of samples was determined using a CTA449C simultaneous thermal analysis setup in a magnetic field. The phase composition of samples was determined using a Rigaku Ultima IV diffractometer with Bragg–Brentano focusing, based on CuK_α radiation with a diffracted-beam graphite monochromator. Point-by-point scanning mode was used; the 2θ angular range was 20°—140°, the step was 0.05. The unit cell parameters of hexaferrites were calculated by interplane distances.

3. RESULTS AND DISCUSSION

The Mössbauer spectra of hexaferrite $BaFe_{12-x}Ti_xO_{19}$ samples are shown in Fig. 1. All spectra were expanded into sextets and doublets using the Univem Ms program. The expansion model was set from the following considerations. In substituted ferrites, sextets belonging to iron ions of main five sites with parameters of unsubstituted hexaferrite were separated, and positions of additional sextets and doublets were visually determined. The best processing version was determined by the minχ^2 parameter while retaining the physical meaning of Mössbauer parameters. Decreases in total intensities of sextet peak positions were used to determine structure sites occupied by impurity ions and broken magnetic couplings of the indirect Fe–O–Fe magnetic exchange. In this case, it was taken into account that nonequivalent sites of Fe ions in the case of substituting ion sites $2a$, $2b$, $4f_1$, and $4f_2$ can be formed in the neighboring polyhedra with which exchange magnetic couplings are broken, and only impurity ion incorporation into site $12k$ can form nonequivalent sites $12k'$ due to joining three octahedra $12k$.

According to these considerations, the Mössbauer spectra of samples with $x = 0.25$ and 0.50 were expanded to 6 sextets, and the spectrum of the sample with $x = 0.75$ was expanded to 7 sextets. An additional doublet appeared in the spectrum of the sample with $x = 1.0$; the spectra of samples with $x = 1.25$ and 1.5 were expanded to 8 sextets and a doublet. Such an expansion provided the best cases of the Pearson criterion min χ^2. In this case, an increase in x was accompanied not only by an increase in the number of sextets in experimental spectra, but also an increase in the total intensity of doublets. The obtained parameters of sextets and doublets, i.e., the isomer (chemical) shift δ (mm/s), quadruple splitting Δ (mm/s), the magnetic field at Fe^{57} nuclei, spectrum component areas S (rel %), resonance line width Γ (mm/s), their correspondence with occupied sites, and the angle θ between the sample magnetic moment and γ-radiation vector in the spectrometer are listed in Table 1. For comparison, Table 1 shows the parameters of one of unsubstituted barium hexaferrites. Since the main contribution to additional sextets C6 and C7 is made by nonequivalent ions of site $12k$, they are denoted by $12k'$ and $12k''$.

The appearance of the doublet in the spectrum of the sample with $x = 1$, on the one hand, suggests that titanium ceased incorporation into the hexaferrite $BaFe_{12-x}Ti_xO_{19}$ structure, and its saturation reached; on the other hand, we can see solid solution decomposition and the formation of new iron–titanium phases. Since a doublet is not still observed in hexaferrite with $x = 0.75$, whereas its total intensity is significant at $x = 1$, it can be considered that the limit of bounded isomorphism of $BaFe_{12-x}Ti_xO_{19}$ hexaferrite is in the range $0.75 < x < 1.0$. Furthermore, an antiferromagnetic α-Fe_2O_3 phase is detected in Mössbauer spectra with $x = 1.25$ and $x = 1.5$.

Estimating the Mössbauer parameters of Table 1, we can note variations of the Fe^{3+} ion isomer shift δ of five basic sites (sextets 1–5) for both unsubstituted and substituted hexaferrites. Comparisons show high δ for Fe^{3+} ions of octahedral sites $12k$, $4f_2$, and $2a$ (δ = 0.33–0.39 mm/s) in comparison with tetrahedral $4f_1$ and bipiramidal $2b$ sites (δ = 0.23–0.29 mm/s) according to [21]. This is explained by the larger covalence of bonds between iron ions due to the smaller volume of polyhedra $4f_1$ and $2b$. In this case, the quadruple splitting Δ of Fe ions increases due to a larger deviation of octahedron $12k$ symmetry from the ideal one. In this case, only ligands contribute to the electric field gradient [22, 23]. In this regard, noteworthy are significant distortions of polyhedron $2b$ symmetry (Δ = 2.07–2.23 mm/s), whereas Δ varies within 0.1–0.18 mm/s for the most symmetric octahedron $2a$.

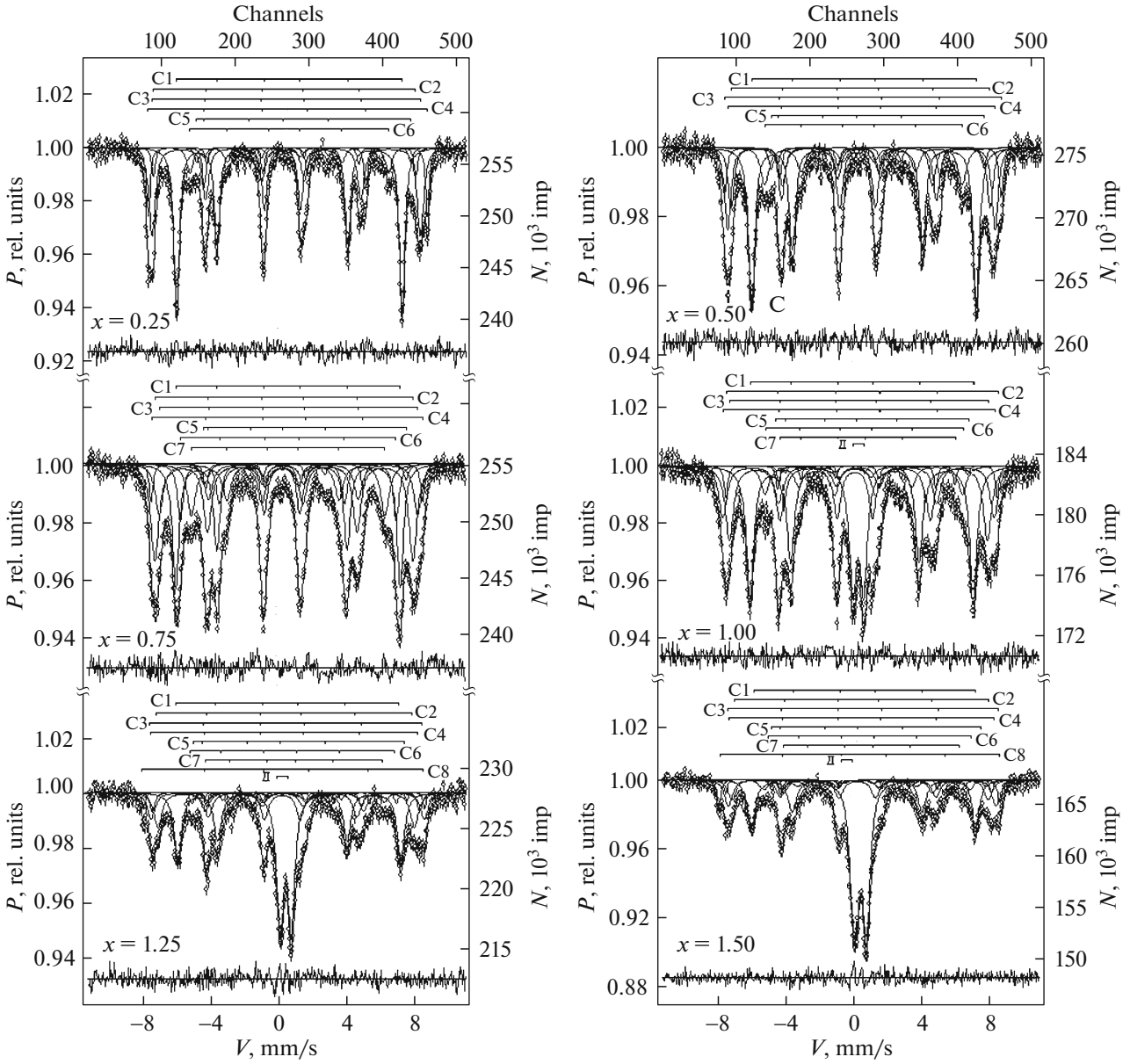

Fig. 1. Mössbauer spectra of *M*-type hexagonal ferrites $BaFe_{12-x}Ti_xO_{19}$ ($x = 0.25$, 0.5, 0.75, 1.00, 1.25, 1.50).

A significant increase in δ additional sextets can be explained, on the one hand, by a decrease in the bond covalence of Fe^{3+} ions, when octahedron 12*k* donates iron ions for the formation of iron–titanium structures and the formation of cation vacancies in this case. This was accompanied by an increase in interaction distances in the triad of octahedra 12*k*, which results in strengthening the ionic bond. In this case, the density of *P*-electrons decreases due to an increase in the screening effect of *d*-electrons with the result of increasing isomer shift.

At the same time, of interest is the implementation scheme of the charge balance in hexaferrite with isomorphic titanium. The classical substitution scheme $2Fe^{3+} \rightarrow Ti^{4+} + Fe^{2+}$ involves divalent iron which should be recorded using Mössbauer spectroscopy. Ions completely satisfying the Fe^{2+} state in the range $0.25 \le x \le 0.75$ were not detected; however, a small increase in δ of Fe sextets C6 (12*k*') with respect to C1 (12*k*) of unsubstituted hexaferrite takes place. A significant increase in δ is observed in additional sextets at $x \rightarrow 1.0$. For example, in the sample with $x = 1.0$, sextet C6 with $\delta = 0.44$ mm/s, appears in the spectrum; at $x = 1.25$, sextets C6 with $\delta = 0.50$ mm/s and C7 with $\delta = 0.56$ mm/s appear; and at $x = 1.5$, sextet with $\delta = 0.63$ mm/s appears (Table 1).

It cannot be considered that formed ions completely satisfy the Fe^{2+} state, since, as shown in the

Table 1. Parameters of Mössbauer spectra of titanium-substituted hexaferrites

Sample $BaFe_{12-x}Ti_xO_{19}$	Spectral component	Isomer shift δ, mm/s	Quadruple splitting Δ, mm/s	Magnetic fields H_{eff}, kOe	Component areas S, rel. %	Line width Γ, mm/s	Angle θ, deg
$x = 0$	C1-12k $(Fe^{3+})_{VI}$	0.35	0.42	414	50.5	0.32	54.9
	C2-4f_1 $(Fe^{3+})_{IV}$	0.26	0.22	491	19.8	0.31	
	C3-4f_2 $(Fe^{3+})_{VI}$	0.38	0.20	516	16.8	0.29	
	C4-2a $(Fe^{3+})_{VI}$	0.34	0.01	507	7.5	0.26	
	C5-2b $(Fe^{3+})_{V}$	0.30	2.21	400	5.3	0.30	
$x = 0.25$	C1-12k $(Fe^{3+})_{VI}$	0.35	0.40	412	43.8	0.39	55.2
	C2-4f_1 $(Fe^{3+})_{IV}$	0.23	0.13	486	21.1	0.44	
	C3-4f_2 $(Fe^{3+})_{VI}$	0.36	0.22	490	12.3	0.44	
	C4-2a $(Fe^{3+})_{VI}$	0.39	0.17	510	12.0	0.38	
	C5-2b $(Fe^{3+})_{V}$	0.29	2.23	392	3.2	0.26	
	C6-12k' $(Fe^{3+})_{VI}$	0.42	0.26	362	7.6	0.34	
$x = 0.50$	C1-12k $(Fe^{3+})_{VI}$	0.36	0.38	410	40.2	0.45	52.0
	C2-4f_1 $(Fe^{3+})_{IV}$	0.26	0.19	472	15.4	0.44	
	C3-2a $(Fe^{3+})_{VI}$	0.38	0.18	505	8.4	0.31	
	C4-4f_2 $(Fe^{3+})_{VI}$	0.33	0.14	488	19.9	0.44	
	C5-2b $(Fe^{3+})_{V}$	0.22	2.22	387	3.5	0.31	
	C6-12k' $(Fe^{3+})_{VI}$	0.37	0.31	360	12.6	0.61	
$x = 0.75$	C1-12k $(Fe^{3+})_{VI}$	0.36	0.3	409	30.8	0.47	53.5
	C2-4f_1 $(Fe^{3+})_{IV}$	0.26	0.09	473	21.5	0.56	
	C3-4f_2 $(Fe^{3+})_{VI}$	0.38	0.29	474	12.7	0.54	
	C4-2a $(Fe^{3+})_{VI}$	0.40	0.12	497	6.4	0.34	
	C5-2b $(Fe^{3+})_{V}$	0.30	2.17	367	2.3	0.29	
	C6-12k' $(Fe^{3+})_{VI}$	0.35	0.32	434	7.1	0.53	
	C7-12k'' $(Fe^{3+})_{VI}$	0.39	0.33	358	19.2	0.77	
$x = 1.00$	C1-12k $(Fe^{3+})_{VI}$	0.36	0.40	408	32.8	0.52	54.9
	C2-4f_2 $(Fe^{3+})_{VI}$	0.41	0.28	497	4.3	0.27	
	C3-4f_1 $(Fe^{3+})_{IV}$	0.28	0.19	473	25.6	0.67	
	C4-2a $(Fe^{3+})_{VI}$	0.35	0.06	498	11.7	0.58	
	C5-2b $(Fe^{3+})_{V}$	0.28	1.94	348	1.1	0.21	
	C6-12k' $(Fe^{3+})_{VI}$	0.44	0.48	360	8.6	0.61	
	C7-12k'' $(Fe^{3+})_{VI}$	0.41	0.97	319	2.2	0.24	
	D-$(Fe^{3+})_{VI}$	0.35	0.63	–	13.7	0.51	

Table 1. (Contd.)

Sample $BaFe_{12-x}Ti_xO_{19}$	Spectral component	Isomer shift δ, mm/s	Quadruple splitting Δ, mm/s	Magnetic fields H_{eff}, kOe	Component areas S, rel. %	Line width Γ, mm/s	Angle θ, deg
$x = 1.25$	C1-12k $(Fe^{3+})_{VI}$	0.36	0.40	409	29.4	0.53	53.8
	C2-4f_1 $(Fe^{3+})_{IV}$	0.28	0.20	470	17.1	0.60	
	C3-4f_2 $(Fe^{3+})_{VI}$	0.39	0.25	503	7.3	0.53	
	C4-2a $(Fe^{3+})_{VI}$	0.33	0.13	491	9.3	0.40	
	C5-2b $(Fe^{3+})_{V}$	0.23	2.07	387	1.2	0.21	
	C6-12k' $(Fe^{3+})_{VI}$	0.50	0.72	375	2.5	0.27	
	C7-12k'' $(Fe^{3+})_{VI}$	0.56	0.77	323	5.1	0.56	
	C8-α-Fe_2O_3	0.37	−0.23	515	3.3	0.21	
	D-$(Fe^{3+})_{VI}$	0.35	0.66	–	24.9	0.48	
$x = 1.50$	C1-12k $(Fe^{3+})_{VI}$	0.36	0.39	409	24.7	0.58	55.5
	C2-4f_1 $(Fe^{3+})_{IV}$	0.28	0.12	471	9.8	0.58	
	C3-4f_2 $(Fe^{3+})_{VI}$	0.35	0.26	492	13.7	0.58	
	C4-2a $(Fe^{3+})_{VI}$	0.30	−0.10	489	2.9	0.22	
	C5-2b $(Fe^{3+})_{V}$	0.28	2.15	395	1.3	0.21	
	C6-12k' $(Fe^{3+})_{VI}$	0.43	0.56	374	4.9	0.58	
	C7-12k'' $(Fe^{3+})_{VI}$	0.65	0.65	327	2.8	0.37	
	C8-α-Fe_2O_3	0.38	−0.17	517	6.2	0.31	
	D-$(Fe^{3+})_{VI}$	0.39	0.67	–	33.7	0.51	

study [21] on systematization of valence and coordination states of Fe^{2+} ions, δ for Fe^{2+} in the environment of O^{2-} should be within 0.94 ± 0.02 mm/s for tetrahedral sites and 1.14 ± 0.02 mm/s for octahedral sites. However, if we assume that the electron exchange $Fe^{3+} \rightarrow Fe^{2+}$ occurs in the spinel block of hexaferrite in octahedra 12k as that in magnetite established in [24], the isomer shift for Fe ions of octahedral sites of magnetite in Mössbauer spectra should be 0.67 mm/s which was established in numerous studies of magnetite. In the sample with $x = 1.5$, the isomer shift of Fe^{3+} ions is 0.65 mm/s, which is relatively close to 0.67 mm/s as in unsubstituted magnetite during electron exchange.

From this we can conclude that only a partial electron exchange occurs with increasing 3d-electron density at small substitutions of Fe^{3+} with Ti^{4+} ions in the spinel block of hexaferrite, whereas the electron exchange mechanism $Fe^{3+} \leftrightarrow Fe^{2+}$ similar to that in magnetite is implemented at $x > 1.0$. The relatively close coincidence of the isomer shift in additional sextets at $x = 1.5$ with that observed in magnetite for octahedral sites points to the high probability of the explanation of an increase in the isomer shift by the electron exchange at the 12k site of hexaferrite, rather than the model of strengthening the ionic bond, which cannot provide the observed increase in the isomer shift in additional sextets of the Mössbauer spectrum.

In contrast to magnetite, where Δ of Fe ions is zero during electron exchange due to the high octahedron symmetry, in hexaferrite $BaFe_{12-x}Ti_xO_{19}$, due to the defect structure formation, local distortions of the octahedron are rather strong, and Δ reaches 0.5 mm/s, which is unrelated to electron exchange.

Magnetic fields at Fe^{57} nuclei monotonically decrease with increasing x. Comparing sextet areas, a certain deviation of areas in tetrahedral sites in the bipyramid from theoretical values can be noted (see Table 1). It can be explained by different vibration amplitudes of Fe ions in these polyhedra.

The smaller vibration amplitude of Fe ions in tetrahedra in comparison with octahedra enhances the res-

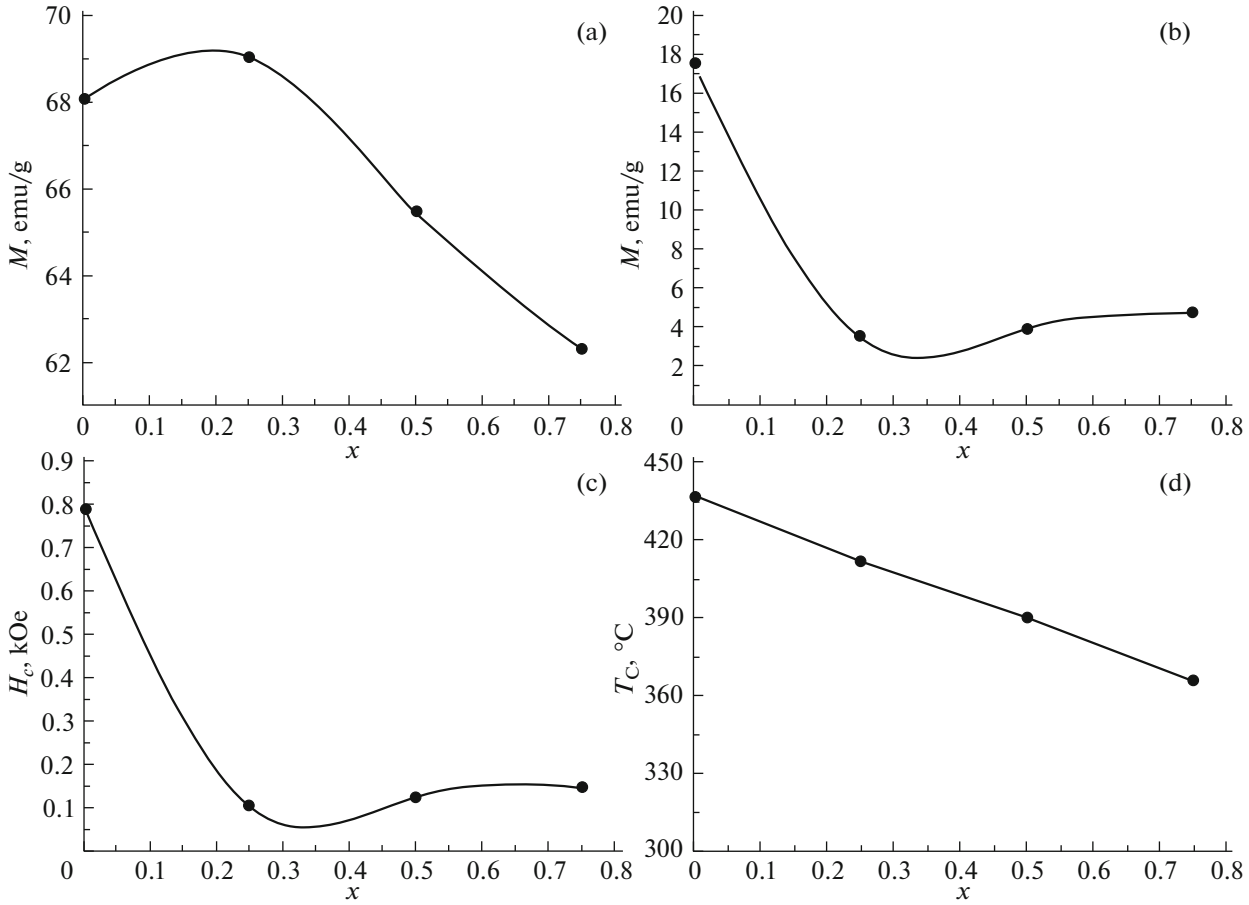

Fig. 2. Dependences of $BaFe_{12-x}Ti_xO_{19}$ magnetic characteristics on x: (a) specific magnetization M_s, emu/g; (b) coercive force H_c, kOe; (c) remanent magnetization M_r, emu/g; and (d) Curie temperatures T_C, °C.

onant effect, hence, increases the area from these ions, and the large amplitude of Fe ion vibrations in the bipyramid in one of the directions decreases the resonant effect.

A comparison of the angle θ of $BaFe_{12-x}Ti_xO_{19}$ samples with x confirms that all samples are almost isotropic.

The measured magnetic characteristics of the samples studied in the x range from 0 to 0.75 of the specific magnetization M, remanent magnetization M_r, coercive force H_c, and Curie temperature T_C in the form of dependences on the degree of substitution x are shown in Fig. 2. The specific magnetization (Fig. 2a) increases from 68 emu/g of unsubstituted hexaferrite to 69 emu/g at $x = 0.25$, and then monotonically decreases to 62 emu/g at $x = 0.75$. This results from the fact that the substitution at the initial stage occurs mostly at the site $4f_2$, increasing the resulting magnetic moment, and then substitutions $12k$ and $2b$ prevail (see Table 1), which decrease the resulting magnetic moment, hence, the specific magnetization, which corresponds to the data [17]. The coercive force and remanent magnetization behave identically, decreasing from the values of unsubstituted hexaferrite to the values at $x = 0.25$, and then they remain almost unchanged to $x = 0.75$. The Curie temperature measured using simultaneous thermal analysis of hexaferrites in a magnetic field (Fig. 2d) showed a decreasing linear dependence.

The field dependences of the magnetization (Fig. 3a) and scaled-up fragments (Fig. 3b) for unsubstituted hexaferrite and compositions with x to 0.75 showed their certain difference. It may be noted that complete magnetization saturation was not reached in the measured range of $B(T)$; we can see two groups of hysteresis loops: loops with higher ($x = 0$, 0.25, 0.5) and lower ($x = 0.75$) specific magnetizations. Furthermore, hysteresis loops of the sample with $x = 0.25$ are closer to rectangularity, which is consistent with the magnetization peak (Fig. 2a).

Using a simultaneous thermal analysis, thermal characteristics of samples with $x = 0$–0.75 were measured; the dependences of differential scanning calorimetry (DSC) and mass loss (thermogravimetry, TG) in a magnetic field obtained at the same time are

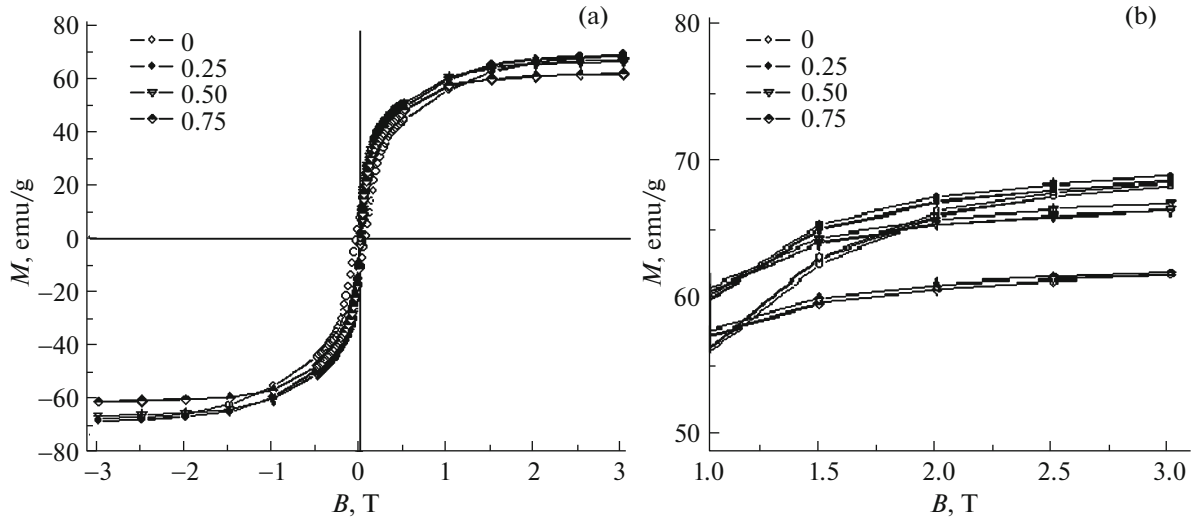

Fig. 3. (a) Hysteresis loops of hexaferrite $BaFe_{12-x}Ti_xO_{19}$; (b) the scaled-up portion with $B = 1–3$.

shown in Fig. 4. Endothermic effects associated with the sample transition from the magnetically ordered ferrimagnetic state to the paramagnetic state are indicated in all curves; therewith, the transition temperature decreases strictly linearly from 452.4 to 371.3°C. The same dependence is reflected by the TG curve measured in a magnetic field (Fig. 2d). In this case, during the transition of the magnetically ordered sample at the Curie temperature, a signal step appears in the temperature dependence of TG, by which the transition temperature can be determined. To compare the effect of the magnetic field on the TG signal, the sample with $x = 0.25$ was measured without magnetic field, where the transition signal in the TG curve is absent. Graphically, the signal in the TG curve is less smeared than the endothermic peak; therefore, the determination of the Curie temperature is more accurate in this case.

The phase composition of samples with $x = 0–0.75$, 1.25, and 1.5 was determined by X-ray diffraction patterns (Fig. 5); the unit cell parameters of hexaferrites calculated by interplane distances are listed in Table 2.

We can see in Table 2 that samples in the composition range $x = 0–0.75$ inclusive represent a $BaFe_{12-x}Ti_xO_{19}$ monofractions.

This suggests that titanium isomorphically enters the hexaferrite lattice within this range. Beginning with $x = 1.0$, the X-ray diffraction data establish the appearance of various iron–titanium compounds

Table 2. $BaFe_{12-x}Ti_xO_{19}$ unit cell parameters and phase composition of samples

Sample $BaFe_{12-x}Ti_xO_{19}$	Hexaferrite unit cell parameters				Phase composition, %
	a, Å	b, Å	c, Å	V, Å^3	
$x = 0$	5.8941(9)	5.8941(9)	23.202(4)	698.06(18)	$BaFe_{12}O_{19}$-100
$x = 0.25$	5.8870(9)		23.1734(13)	695.52(16)	$BaFe_{11.75}Ti_{0.25}O_{19}$-100
$x = 0.50$	5.888(3)		23.225(15)	697.41(7)	$BaFe_{11.5}Ti_{0.5}O_{19}$-100
$x = 0.75$	5.870(4)		23.2447(12)	697.66(8)	$BaFe_{11.25}Ti_{0.75}O_{19}$-100
$x = 1.0$	5.8858(4)		23.2307(18)	699.93(9)	$BaFe_{11.25}Ti_{0.75}O_{19}$-95.1, Fe_2TiO_4-2, $FeTiO_3$-2.5
$x = 1.25$	5.8886(6)		23.232(2)	697.65(12)	$BaFe_{11.25}Ti_{0.75}O_{19}$-81, Fe_3O_4-12, TiO_2-7.2
$x = 1.50$	5.886(8)		23.219(11)	696.65(17)	$BaFe_{11.25}Ti_{0.75}O_{19}$-70.2, Fe_3O_4-5.2, $FeTiO_3$-2.9, Ti_2O_4-9.4, TiO_2-14.7 Ti_2O_3-0.5

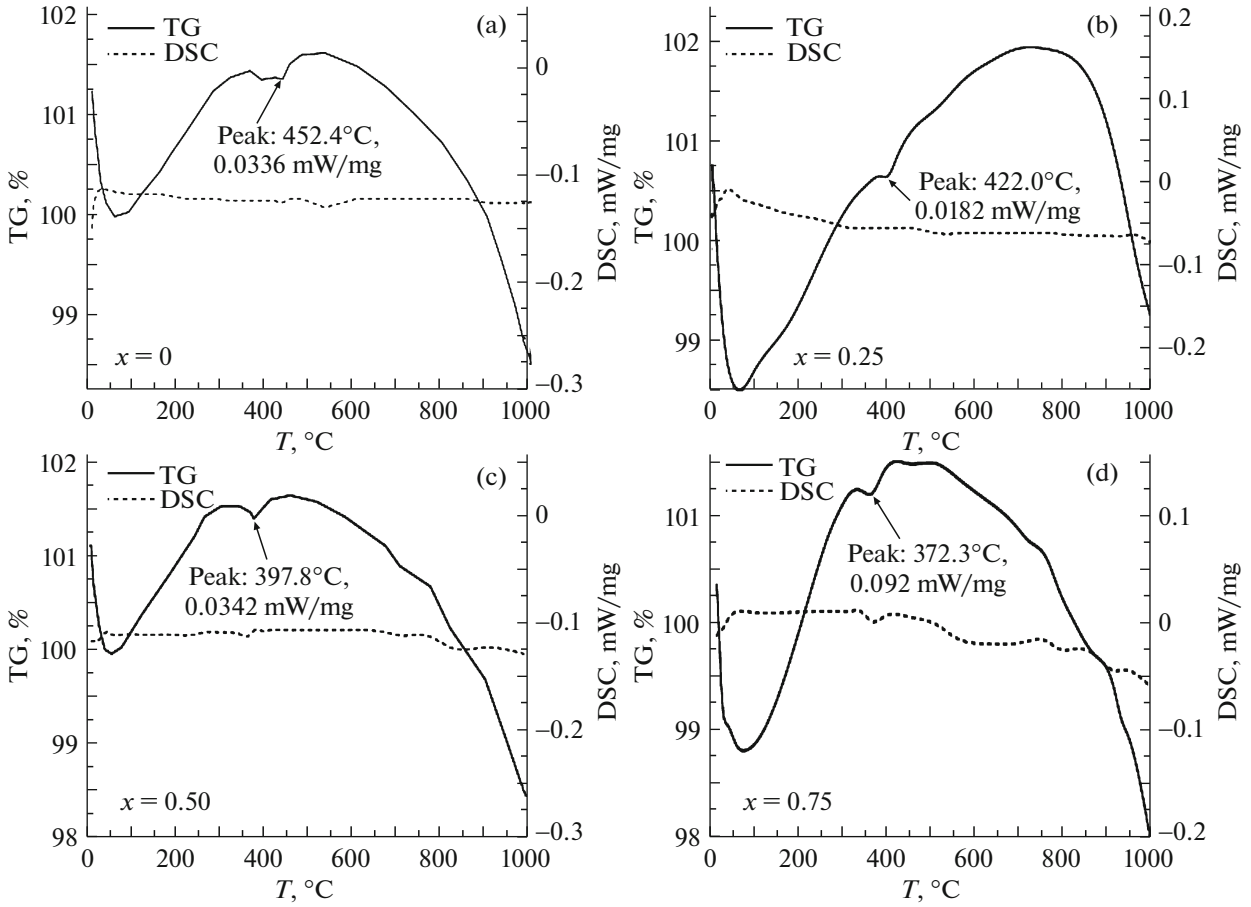

Fig. 4. Curves of differential scanning calorimetry (DSC) and mass loss (thermogravimetry, TG) of $BaFe_{12-x}Ti_xO_{19}$ hexaferrites ($x = 0$, 0.25, 0.50, 0.75).

(Table 2) at an almost unchanged composition of hexaferrite $BaFe_{11.25}Ti_{0.75}O_{19}$. This indicates bounded isomorphism of hexaferrite and isomorphism limit in the range $0.75 < x < 1.0$, which is consistent with the Mössbauer spectroscopy data showing the absence of a doublet in the spectra of samples with $x = 0.75$ and the doublet appearance at $x = 1.0$.

The calculated $BaFe_{12-x}Ti_xO_{19}$ unit cell parameters (Table 2) show that the titanium incorporation into the lattice decreases the parameter a in the composition with $x = 0.25$ with respect to unsubstituted hexaferrite, but a further increase in x does not affect this parameter. In contrast to the parameter a, the parameter c and unit cell volume V show maxima in the range of 0.75–1.0, which can also be associated with reaching the isomorphism limit.

4. CONCLUSIONS

The performed study showed that bounded heterovalent isomorphism according to the scheme $2Fe^{3+} \rightarrow Ti^{4+} + Fe^{2+}$ takes place in titanium-alloyed barium hexaferrite. It was found that the limit of heterovalent isomorphic substitution in $BaFe_{12-x}Ti_xO_{19}$ is in the range of $0.75 < x < 1.0$; then, titanium in compound with iron, separated from sites 12k and 2b, forms paramagnetic ulveshpinel, magnetite, and titanium dioxide according to the X-ray diffraction and Mössbauer spectroscopy data. In samples with $x = 1.25$ and 1.5, iron oxide α-Fe_2O_3 was determined by Mössbauer parameters. The formation of iron–titanium compounds and titanium dioxide is detected at $x = 1.0$, and their content increases with x. The electron exchange $Fe^{3+} \leftrightarrow Fe^{2+}$ in the range $x = 1.0$–1.5 in the spinel block of the $BaFe_{12-x}Ti_xO_{19}$ structure was detected by the isomer shift similar to that observed in magnetite. Additional sextets in Mössbauer spectra of barium hexaferrite can be formed in the case of Ti^{4+} ion localized mostly at sites 12k and 2b, due to broken exchange couplings Fe(12k)–O–Fe(12k), Fe(4f_2)–O–Fe(12k), Fe(2a)–O–Fe(12k), and Fe(4f_2)–O–Fe(2b) denoted by 12k' and 12k".

The dependence of the specific magnetization of $BaFe_{12-x}Ti_xO_{19}$ exhibited a maximum at $x = 0.25$ due to the prevalence of the substitution at the site 4f_2,

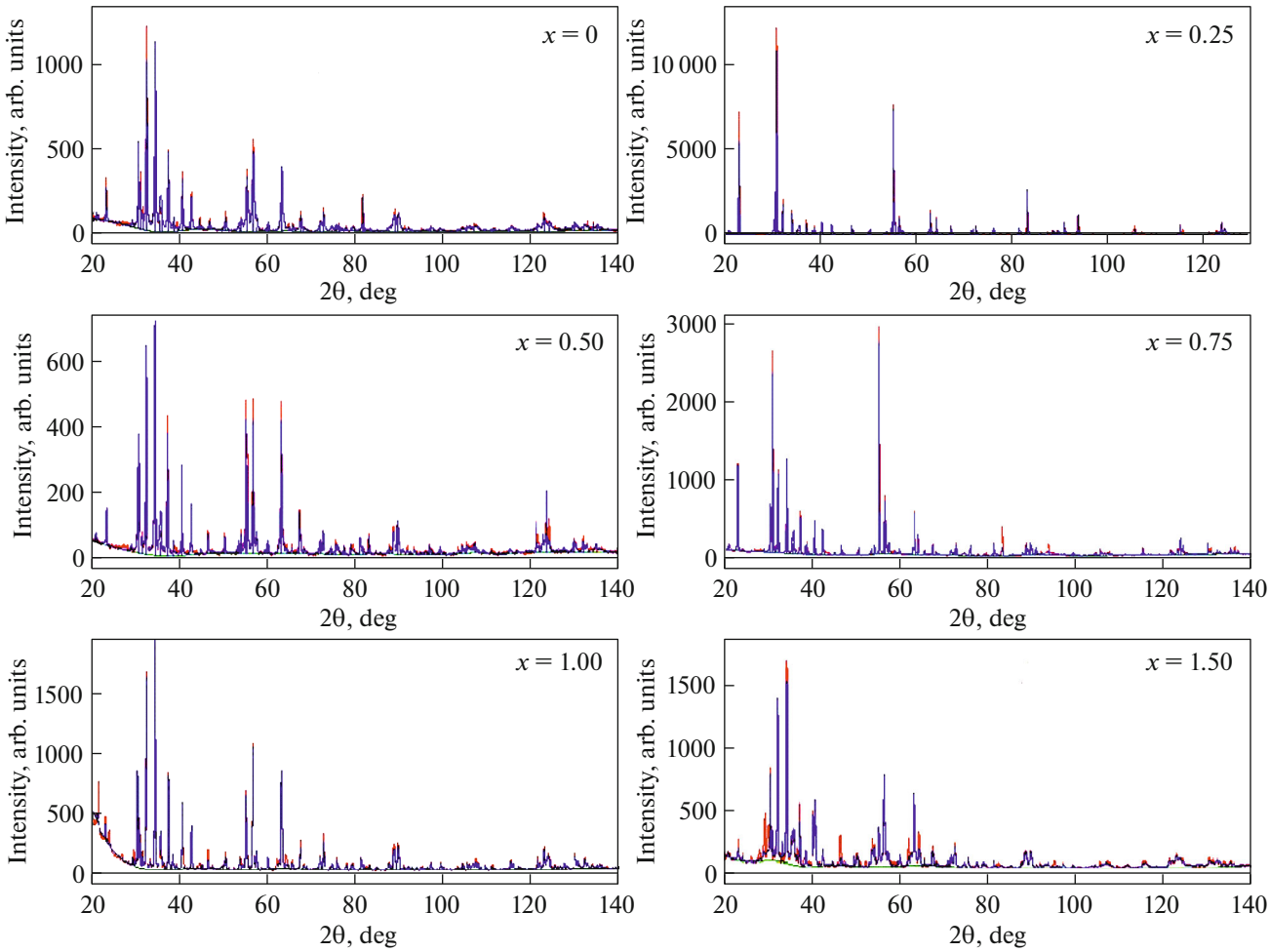

Fig. 5. X-ray diffraction patterns of hexaferrites $BaFe_{12-x}Ti_xO_{19}$ ($x = 0$, 0.25, 0.50, 0.75, 1.00, 1.50).

after which the magnetization monotonically decreases with increasing x.

The studies performed show the application ranges of titanium-substituted barium hexaferrite and the possibility of obtaining samples with prescribed magnetic properties for industrial applications.

FUNDING

This study was supported by the Russian Science Foundation, agreement no. 19-19-00694, May 6, 2019.

CONFLICT OF INTEREST

The authors declare that they have no conflicts of interest.

REFERENCES

1. V. Adelskold, Ark. Mineral. Geol. A **12**, 1 (1938).
2. R. C. Pullar, Prog. Mater. Sci. **57**, 1191 (2012).
3. J. Smit and H. P. J. Wijn, *Ferrites* (Phylips Tech. Lib., 1959).
4. V. V. Korovushkin, M. N. Shipko, V. G. Kostishin, I. M. Isaev, A. Yu. Mironovich, S. V. Trukhanov, and A. V. Trukhanov, Inorg. Mater. **55**, 1007 (2019).
5. A. S. Kamzin and L. P. Ol'khovik, Phys. Solid State **41**, 1658 (1999).
6. V. V. Korovushkin, A. V. Trukhanov, M. N. Shipko, V. G. Kostishin, I. M. Isaev, A. Yu. Mironovich, and S. V. Trukhanov, Russ. J. Inorg. Chem. **64**, 574 (2019).
7. A. V. Trukhanov, V. G. Kostishin, V. V. Korovushkin, L. V. Panina, S. V. Trukhanov, V. A. Turchenko, I. S. Polyakov, R. Kh. Rakhmatulin, G. A. Filatov, T. I. Zubar', V. V. Oleinik, E. C. Yakovenko, L. Yu. Matsui, L. L. Vovchenko, V. L. Launets, and E. L. Rukhanova, Phys. Solid State **60**, 1768 (2018).
8. Sh. Sh. Bashkirov, A. V. Liberman, A. A. Valiulin, L. D. Zaripova, and S. V. Kokin, Phys. Solid State **42**, 79 (2000).
9. T. Tsutaoka, A. Tsurunaga, and N. Koga, J. Magn. Magn. Mater. **399**, 64 (2016).
10. M. H. Shams, A. Rozatian, M. Yousefi, J. Valiček, and V. Šepelák, J. Magn. Magn. Mater. **399**, 10 (2016).
11. V. V. Somana, V. M. Nanotib, D. K. Kulkarnic, and V. V. Somand, Phys. Proc. **54**, 30 (2014).

12. A. Ghasemi, A. Hossienpour, A. Morisako, A. Saatchi, and M. Salehi, J. Magn. Magn. Mater. **302**, 429 (2006).
13. R. Alam, M. Tehrani, M. Moradi, E. Hosseinpour, and A. Sharbati, J. Magn. Magn. Mater. **323**, 1040 (2011).
14. Y. Zheng, Z. Yu, Y. Shao, S. Mo, and Y. Lin, Hyperfine Interact. **94**, 2035 (1994).
15. R. Alam, M. Moradi, H. Nikmanesh, J. Ventura, and M. Rostami, J. Magn. Magn. Mater. **402**, 20 (2016).
16. C. L. Lengauer, E. Tillmans, and G. Hentschel, Mineral. Petrol. **71**, 1 (2001).
17. P. A. Mariño-Castellanos, J. Anglada-Rivera, A. Cruz-Fuentes, and R. Lora-Serrano, J. Magn. Magn. Mater. **280**, 214 (2004).
18. P. Quoiroz, B. Halbedel, A. Bustamante, and J. Gonzalez, Hyperfine Interact. **202**, 97 (2011).
19. D. A. Vinnik, D. A. Zherebtsov, L. S. Mashkovtseva, A. S. Semisalova, I. V. Krivtsov, L. I. Isaenko, G. G. Mikhailov, and R. Niewa, Cryst. Growth Des. **14**, 5834 (2014).
20. D. A. Vinnik, D. A. Zherebtsov, L. S. Mashkovtseva, N. S. Perov, A. S. Semisalova, I. V. Krivtsov, L. I. Isaenko, and G. G. Mikhailov, in *Proceedings of the 6th Baikal International Conference, 2014*, p. 161.
21. F. Menil, J. Phys. Chem. Solids **46**, 763 (1985).
22. R. Ingalls, Phys. Rev. A **133**, 787 (1964).
23. G. Bancroft, A. Maddock, and R. Burns, Geochim. Cosmochim. Acta **31**, 2219 (1967).
24. E. J. W. Verwey and P. H. Haaman, Physica (Amsterdam, Neth.) **8**, 979 (1941).

Translated by A. Kazantsev